Author Manuscript

Author Manuscript

Author Manuscript

Author Manuscript

HHS Public Access

Author manuscript

Nat Biomed Eng. Author manuscript; available in PMC 2019 March 12.

Published in final edited form as:

Nat Biomed Eng. 2018 November ; 2(11): 810–821. doi:10.1038/s41551-018-0275-1.

Alginate encapsulation as long-term immune protection of allogeneic pancreatic islet cells transplanted into the omental bursa of macaques

Matthew A. Bochenek[#1,2,3,4,5], **Omid Veiseh**[#3,4,5,+], **Arturo J. Vegas**[3,4,5,++], **James J. McGarrigle**[1], **Meirigeng Qi**[1], **Enza Marchese**[1], **Mustafa Omami**[1], **Joshua C. Doloff**[3,4,5], **Joshua Mendoza-Elias**[1,2], **Mohammad Nourmohammadzadeh**[1,2,+++], **Arshad Khan**[1], **Chun-Chieh Yeh**[1], **Yuan Xing**[1,2,§], **Douglas Isa**[1], **Sofia Ghani**[1], **Jie Li**[3,4,5,+], **Casey Landry**[3,4,5], **Andrew R. Bader**[3,4,5], **Karsten Olejnik**[3,4,5,+], **Michael Chen**[3,4,5], **Jennifer Hollister-Lock**[6], **Yong Wang**[1,2,§], **Dale L. Greiner**[7], **Gordon C. Weir**[6], **Berit Løkensgard Strand**[11], **Anne Mari A. Rokstad**[12,13], **Igor Lacik**[14], **Robert Langer**[3,4,5,8,9,10], **Daniel G. Anderson**[3,4,5,8,9,10,#], and **Jose Oberholzer**[1,2,§,#]

[1]Division of Transplantation, Department of Surgery, University of Illinois at Chicago, 840 South Wood Street, Chicago, IL 60612, USA

[2]Department of Bioengineering, University of Illinois at Chicago, 851 South Morgan Street, Chicago, IL 60607, USA

[3]David H Koch Institute for Integrative Cancer Research, Massachusetts Institute of Technology, 500 Main Street, Cambridge, MA 02139, USA

[4]Department of Chemical Engineering, Massachusetts Institute of Technology, 77 Massachusetts Avenue, Cambridge, MA 02139, USA

Users may view, print, copy, and download text and data-mine the content in such documents, for the purposes of academic research, subject always to the full Conditions of use: http://www.nature.com/authors/editorial_policies/license.html#terms

For correspondence: Dan Anderson: dgander@mit.edu; Tel.: +1 617 258 6843; fax: +1 617 258 8827, or, Jose Oberholzer: JO5JE@hscmail.mcc.virginia.edu; Tel.: +1 434 243 3951; fax: +1 434 924 5539.

[+]Present address: Sigilon Therapeutics, Inc., 161 First St., Cambridge, MA 02142, USA and Department of Bioengineering, Rice University, Houston, TX 77005, USA

[++]Present address: Chemistry Department, Boston University, 590 Commonwealth Ave., Boston, MA 02215, USA

[+++]Present address: Department of Chemical and Biomolecular Engineering, North Carolina State University, 911 Partners Way, Raleigh, NC 27606, USA

[§]Present address: Department of Surgery and Biomedical Engineering, University of Virginia, PO Box 800709, Charlottesville, VA 22908, USA

Author Contributions:

M.A.B., O.V., A.J.V., J.J.M., D.G.A., and J.O. designed experiments, analyzed data and wrote the manuscript. M.A.B., O.V., A.J.V., J.J.M., M.Q., E.M., M.O., J.C.D., J.E.M., M.N., A.K., C.C.Y., D.I., S.G., J.L., C.L., A.R.B., K.O., M.C., Y.W., and J.O. performed experiments. J.H.L., D.L.G., G.C.W., B.L.S., A.A.R., I.L., and R.L. provided conceptual advice and technical support. R.L., D.G.A., and J.O. supervised the study. All of the authors discussed the results and assisted in the preparation of the manuscript.

Additional Information:

Correspondence should be addressed to Dr. Jose Oberholzer and any material requests should be addressed to Dr. Dan Anderson.

Competing Financial Interests:

O.V., A.J.V., R.L., D.G.A., and J.O. are founding scientists of Sigilon Therapeutics, Inc. a biotech company based in Cambridge, MA, USA that produces anti-fibrotic materials for cell-based therapies. J.O. is founder and President of CellTrans Inc. a biotech company based in Chicago, IL, USA for the transplantation of cell based therapies.

Data availability:

The datasets generated and/or analyzed during this study are available from the corresponding author on reasonable request.

Author Manuscript Author Manuscript Author Manuscript Author Manuscript

[5]Department of Anesthesiology, Boston Children's Hospital, 300 Longwood Ave, Boston, MA 02115, USA

[6]Section on Islet Cell and Regenerative Biology, Research Division, Joslin Diabetes Center, One Joslin Place, Boston, MA 02215, USA

[7]Program in Molecular Medicine, University of Massachusetts Medical School, Worcester, MA 01605, USA

[8]Howard Hughes Medical Institute, Harvard University, Cambridge, MA 02138, USA

[9]Division of Health Science Technology, Massachusetts Institute of Technology, 77 Massachusetts Avenue, Cambridge, MA 02139, USA

[10]Institute for Medical Engineering and Science, Massachusetts Institute of Technology, 77 Massachusetts Avenue, Cambridge, MA 02139, USA

[11]Department of Biotechnology and Food Sciences, Norwegian University of Science and Technology, Trondheim, Norway

[12]Department of Cancer Research and Molecular Medicine, Norwegian University of Science and Technology, Trondheim, Norway

[13]Centre of Obesity, Clinic of Surgery, St. Olavs University Hospital, Trondheim, Norway

[14]Polymer Institute, Slovak Academy of Sciences, Bratislava, Slovakia

[#] These authors contributed equally to this work.

Abstract

The transplantation of pancreatic islet cells could restore glycaemic control in patients with type-I diabetes. Microspheres for islet encapsulation have enabled long-term glycaemic control in diabetic rodent models; yet human patients transplanted with equivalent microsphere formulations have experienced only transient islet-graft function, owing to a vigorous foreign-body reaction (FBR), to pericapsular fibrotic overgrowth (PFO) and, in upright bipedal species, to the sedimentation of the microspheres within the peritoneal cavity. Here, we report the results of the testing, in non-human primate (NHP) models, of seven alginate formulations that were efficacious in rodents, including three that led to transient islet-graft function in clinical trials. Although one month post-implantation all formulations elicited significant FBR and PFO, three chemically modified, immune-modulating alginate formulations elicited reduced FBR. In conjunction with a minimally invasive transplantation technique into the bursa omentalis of NHPs, the most promising chemically modified alginate derivative (Z1-Y15) protected viable and glucose-responsive allogeneic islets for 4 months without the need for immunosuppression. Chemically modified alginate formulations may enable the long-term transplantation of islets for the correction of insulin deficiency

---

Cell encapsulation within semi-permeable hydrogels represents a local immunoisolation strategy for cell-based therapies without the need for systemic immunosuppression[1,2]. Applied to islets of Langerhans transplantation, this concept represents a functional cure for patients afflicted with insulin dependent diabetes[2]. The hydrogel sphere allows for diffusion

Author Manuscript Author Manuscript Author Manuscript Author Manuscript

of insulin and nutrients necessary for cell function while excluding immune cells that would reject the foreign cells. Alginate spheres have been one of the most widely investigated cell encapsulation materials as this anionic polysaccharide forms a hydrogel in the presence of divalent cations under cell friendly conditions. This natural co-polymer can then exhibit differential physical properties depending on the ratio and sequential arrangement of mannuronic (M) and guluronic (G) acid residues, molecular weight, concentration, and divalent cations used to form the gels[3]. For instance, a high G-block content alginate has a higher binding affinity for barium ions and will form a tighter, more stable network compared to the same alginate type cross-linked with calcium[4]. Additionally, electrostatic complexation of a positively charged polymer to the negatively charged alginate surface can provide an outer layer to reduce sphere porosity and increase sphere stability[5]. A final outer alginate layer or chemical modification of the polycation used for coating has been investigated to reduce the positive surface charge density of the sphere[5–7]. Many alginate sphere formulations produced with variations in the alginate concentration, cross-linking ion or inclusion/exclusion of a polycation layer have demonstrated long-term diabetes correction in rodent models[8–11]. Unfortunately, these results have not translated at a similar potency when these formulations have been applied to diabetic patients[12–15].

Investigators have reported transient glycemic control and limited therapeutic benefit to the patients[12–15]. These studies suggest that the encapsulated islet cells are not remaining viable post transplantation into the general intraperitoneal (IP) space of humans. Based on the reported clinical observations and experimental animal data, we hypothesized that the major contributing factors to loss of cell function included pericapsular fibrotic overgrowth (PFO), sphere aggregation, and inadequate metabolite supply of the transplantation site[14–20]. PFO results from a foreign body reaction to the implantable material with deposition of an extra-cellular matrix (ECM) and cellular network to wall off the foreign entity from the body[21]. This fibrotic network then impacts graft viability by restricting oxygen and metabolite diffusion into the spheres[22]. Clumping of the spheres can further diminish nutrition by increasing exchange distances to the cells housed in the center of the clumps[16,17]. Clumping of the microspheres occurs more commonly in bipedal animals consequent to gravity-based sedimentation into the lowest point of the peritoneal cavity: the Douglas space. The IP transplantation site also has been reported to be a hypoxic environment for islets with low oxygen partial pressures (pO_2) that may not support healthy endocrine function[18].

To test our hypothesis, we chose a non-human primate (NHP) animal model that is bipedal, genetically, immunologically and anatomically more similar to humans than rodents, dogs or pigs, and would provide a better surrogate model prior to testing in humans[23]. Similar to humans, NHP animal models are exposed to diverse sets of antigens compared to inbred rodents raised in sterile environments[24], and the longer life-time of exposure to somatic mutation may allow the immune system of NHPs to better identify and combat distinctive foreign entities within the body[25].

First, we sought to investigate if the NHP model could recapitulate outcomes from human patients transplanted with the same alginate sphere formulations[12–15]. Three alginate formulations, previously tested in human patients with transient encapsulated islet graft function, were formulated without islets and implanted into the general IP space (greater

Author Manuscript Author Manuscript Author Manuscript Author Manuscript

sac) of NHP. Each of the clinical alginate formulations elicited a significant foreign body response and pericapsular fibrotic overgrowth (PFO) in NHP. PFO was described as a major contributor to loss of cell viability in the human patients and illustrates that the NHP model can recapitulate findings from human patients transplanted with the same material formulations. In contrast, three immune modulating alginate formulations (Z1-Y19, Z2-Y12, and Z1-Y15)[26,27] were found to mitigate the foreign body response and PFO in NHP, with two chemically modified formulations (Z2-Y12 and Z1-Y15) being the most effective in prevention of PFO. An alternative transplantation technique into the bursa omentalis (lesser sac of the peritoneal cavity) was then developed to impede sphere clumping, and the most promising Z1-Y15 chemically modified alginate derivative was further evaluated for potential allogeneic islet transplantation in NHPs. When retrieved after 1 month and 4 months post-transplantation, the Z1-Y15 encapsulated islets were free of PFO in six out of seven NHP with a median islet cell viability of 93.5% and 90.0%, respectively. *In vitro* assessments performed on the retrieved Z1-Y15 encapsulated islets indicate functional engrafted endocrine tissue, which further suggests that the bursa omentalis transplantation site (pO_2 levels of 35.0 ± 3.2 mmHg) can support encapsulated islets if devoid of fibrotic overgrowth to ensure free nutritional exchange. Combining these design principles promoted islet viability for the duration of the study (4 months) post transplantation into NHP without the use of any immunosuppression. This work provides the foundation for proof of concept clinical trials with encapsulated, isolated pancreatic islets from deceased organ donors.

Clinical trial alginate formulations elicit FBR in NHP

Each of the sphere formulations used in both the human clinical trials and NHP studies presented here were produced according to the following design criteria (Table 1). In addition, to ensure the microspheres to be as close as possible to the one used in the clinical trials, they were produced by the original inventors after technology transfer to the University of Illinois (A-PLO-A and UPMVG-Ca^{2+}/Ba^{2+}) or shipped from the original lab conducting the clinical trials (UPMVG-Ba^{2+}). The alginate-(poly-L-ornithine)-alginate (A-PLO-A) spheres were produced with a 1.7% wt/vol custom-made highly purified alginate, cross-linked with 109 mM calcium, and an additional polycation layer (poly-L-ornithine) was added to restrict sphere permeability[12,13]. An outer alginate layer was added to reduce the surface positive charge[5]. The UPMVG-Ba^{2+} spheres were produced with a 2.2% wt/vol “ultra-pure medium viscosity high guluronic acid content” alginate composition and cross-linked with 20 mM barium[14]. In comparison to calcium cross-linked alginate spheres, barium spheres have a higher modulus of elasticity, reduced permeability with respect to IgG penetration, and are less susceptible to swelling under osmotic pressure changes[9,28]. The UPMVG-Ca^{2+}/Ba^{2+} spheres were produced with a 1.8% wt/vol “ultra-pure medium viscosity high guluronic acid content” alginate composition and cross-linked with 50 mM calcium and a low concentration of 1 mM barium[15,29]. This divalent cation combination was found to reduce the swelling of calcium alginate spheres under osmotic pressure changes while reducing barium content as free barium can be toxic at high levels[30]. Ca^{2+}/Ba^{2+} spheres are reported to have an intermediate modulus of elasticity with respect to calcium and barium cross-linked spheres, but an IgG permeability equivalent to calcium cross-linked spheres[29]. While each of the sphere formulations implemented in the clinical trials were

Author Manuscript Author Manuscript Author Manuscript Author Manuscript

produced with distinct variations in physical properties such as elastic modulus or permeability, the ideal hydrogel properties that can provide optimal immunoprotection of cells without compromising cell nutrition remains unclear[31].

To mimic the formulations used in the clinical trials[12–15], each of the alginate sphere formulations (A-PLO-A, UPMVG-Ba^{2+}, UPMVG-Ca^{2+}/Ba^{2+}) were produced at the 0.5 mm size without islets and implanted into the general IP space of NHP using a minimally invasive laparoscopic surgery[17]. After 1 week, all three of the clinical alginate sphere formulations began to show signs of cellular attachment (Fig. 1a). By 1 month, each became enveloped in fibrotic tissue that could not be retrieved by repeated peritoneal lavages or mechanical agitation (Fig. 1b). These findings are similar to the reports of the human clinical trials where the spheres were adhered to omental tissue[14,15]. H & E and immunohistochemical staining of retrieved samples show multi-cellular layers surrounding the spheres (Fig. 1a) and were composed of foreign body giant cells, $CD11b^{+}$ myeloid cells, and smooth muscle actin (SMA) positive myofibroblasts (Supplementary Fig. 1); consistent with cellular populations involved in foreign body responses to implantable materials[32]. The majority of the responding $CD11b^{+}$ cells to alginate microspheres also has recently been identified as $CD68^{+}$ macrophages[21]. The three empty sphere formulations (A-PLO-A, UPMVG-Ba^{2+}, UPMVG-Ca^{2+}/Ba^{2+}) elicited similar fibrotic responses post-implantation in NHP compared to the human patients transplanted with the same alginate sphere formulations containing allogeneic islets (Fig. 1a-b).

Chemically modified alginate derivatives reduce FBR in NHP

In contrast to the above clinically tested spheres, a combinatorial approach was taken to apply unique chemical modifications to an alginate polymer backbone in order to identify sphere formulations with reduced fibrotic potential. Of the 774 alginate derivatives created, three lead chemically modified alginate derivatives were found to exhibit anti-fibrotic properties after *in vivo* screening in the C57BL/6J mouse model[26]. This strain of mouse exhibits strong foreign body responses to implantable materials that is similar to fibrotic responses observed in humans[33]. The impact of sphere size was similarly investigated in the C57BL/6J mouse model, and interestingly, 1.5 mm diameter plain alginate spheres were determined to illicit less fibrosis following implantation when compared to conventional 0.5 mm diameter spheres[27]. The combination of both the anti-fibrotic alginate and an optimal sphere size was tested with stem cell derived human beta cells, and enabled long-term glycemic control in the diabetic, immune competent C57BL/6J mouse model[34].

We sought to determine whether the anti-fibrotic nature of the chemically modified alginate derivatives and larger sized spheres seen in C57BL/6J mice would translate similarly in NHPs. The chemically modified alginate analogs were synthesized and co-formulated with an unmodified high molecular weight SLG100 alginate as previously reported[26]. Three modified alginate derivatives (Z1-Y19-Ba^{2+}, Z2-Y12-Ba^{2+}, Z1-Y15-Ba^{2+}) and a plain alginate (SLG20-Ba^{2+}) were then formulated as empty spheres at the 1.5 mm size, and evaluated in NHP (Table 1). Contrary to the previous clinical alginate sphere formulations, each of the 1.5 mm sized spheres were easily flushed from the general IP space 1 month post-implantation (Fig. 1c). The amount of PFO coverage of the 1.5 mm spheres was

Author Manuscript Author Manuscript Author Manuscript Author Manuscript

substantially improved compared to previous clinical alginate formulations at the 0.5 mm size, and two chemically modified alginates (Z2-Y12-Ba^{2+}, and Z1-Y15-Ba^{2+}) were found to mitigate the foreign body reaction in NHPs the most effectively (Fig. 1d; Supplementary Table 1).

The bursa omentalis transplantation site

Despite these results, we observed that the modified alginate spheres transplanted near the lobes of the liver within the general IP space (Fig. 2a (I)) tended to descend over time and aggregate in the Douglas space (base of peritoneal cavity) (Fig. 2a (II)). It has been hypothesized that non-fibrosed spheres undergo gravitational sedimentation within the IP space of bipedal animals, which can lead to clumping of encapsulated islets and diminished islet functionality[16,17]. Clumping of encapsulated islets was further noted as a potential cause for graft failure in the clinical trials[15]. To avoid this, we sought to develop methods to impede settling and clumping of encapsulated cell technologies within the Douglas space.

The peritoneal cavity contains discrete compartments separated by layers of peritoneum (Fig. 2). We hypothesized that spheres could be introduced behind the general IP space (greater sac) and into the bursa omentalis compartment (lesser sac); a technique that would constrain the spheres within the tissue bilayer formed by the greater omentum. The friction of the bursa omental folds draping the spheres would then limit sphere movement and clumping. To perform the bursa omentalis transplantation technique, a small incision is introduced laparoscopically into an avascular section of the gastrocolic ligament. Alternatively, the bursa omentalis can be approached via the foramen of Winslow. The spheres are then infused into the bursa omentalis (Fig. 2a (III); Supplementary Video 1). Over time, we observed the spheres would distribute uniformly as a monolayer between the two vascularized omental layers (Fig. 2a (IV); 2b).

pO_2 measurements of alternative transplantation sites

Hypoxia within the IP transplantation site is another proposed cause of encapsulated islet graft failure. The partial pressures of oxygen (pO_2) within the peritoneal cavity may not support healthy endocrine function. However, oxygen measurements of the IP site using small animal models have reported large ranges in pO_2 (15–79 mmHg), and *in situ* pO_2 of islets has been reported at 40 mmHg[35–38]. Due to these discrepancies, we sought to investigate the pO_2 within the IP site as well as select alternative transplantation sites for islets using a more clinically relevant NHP model. Alternative transplantation sites for microencapsulated islets have previously been investigated in rodents and/or NHP including the peritoneal cavity, omental pouch, intrahepatic, kidney capsule, subcutaneous, intramuscular, intra-epididymis, and bone marrow cavity[39–46]. The ideal transplantation site should 1) not produce an acute inflammatory response post-transplantation, 2) be a large enough space to accommodate the encapsulated islet graft, 3) provide sufficient oxygenation/exchange of metabolites, 4) be easily accessible for implantation and retrieval in case of adverse side effects, and 5) facilitate the engraftment process where secreted insulin can be effectively delivered to target tissues for blood glucose homeostasis[47]. Previously investigated sites may be better or worse equipped for each of these parameters.

Author Manuscript Author Manuscript Author Manuscript Author Manuscript

For instance, the subcutaneous site may be the most easily accessible but restricted by the space available to accommodate a large material/cell graft. The peritoneal cavity may provide a large space but be restricted by sedimentation/clumping in the lowest point of the site in bipedal animals hindering nutritional diffusion. We compared the pO_2 of alternative transplantation sites to begin probing the suitability of alternative sites, and identify which may require additional tissue engineering strategies in the future[48].

First, the proper fraction of inspired oxygen (FiO_2) to use during surgical intubation of NHP was determined to ensure the pO_2 measurements of the various transplantation sites adequately recapitulate a NHP breathing normal air (Supplementary Fig. 2). Subsequent steady-state measurements indicate that the average pO_2 levels within the general IP space were indeed lower when compared to the pancreas (30.7 ± 1.6 mmHg vs. 39.6 ± 3.2 mmHg, respectively) (Fig. 2c; Supplementary Table 2). The bursa omentalis showed a trend of increased average pO_2 compared to the general IP space but this was not found to be significantly different (35.1 ± 3.2 mmHg vs 30.7 ± 1.6 mmHg; respectively). The kidney capsule was found to yield the highest pO_2 measurements compared to other sites (48.7 ± 1.3 mmHg). This property may confer the positive function of naked islets post-transplantation compared to other sites in rodents; however, the invasive surgical procedure and organ manipulation seriously hampers human translation of this site[49]. Interestingly, the subcutaneous site yielded higher pO_2 levels than anticipated (39.0 ± 2.1 mmHg); yet, this site in its natural state has not proven to be an effective transplantation site for naked or encapsulated islets[41,46,48].

The bursa transplantation site demonstrated a trend of decreased average pO_2 levels compared to the pancreas (35.1 ± 3.2 mmHg vs 39.6 ± 3.2 mmHg; respectively); although this was not found to be statistically significant (individual *p* values presented in Supplementary Table 3). Normally, *in situ* islets contain a rich microvasculature and fenestration by endothelial cells that is mostly loss during the isolation/encapsulation process, leading to some degree of cell hypoxia especially in the core of the cell clusters[50]. It has been previously reported that exposure of immunoisolated islets to hypoxic conditions *in vitro* can diminish islet function[51]. However, even when reducing the fraction of oxygen from 21% (normoxia) to 10% (hypoxia), encapsulated islets can remain viable and glucose responsive, albeit with a decrease in intracellular signaling of coupling factors important in the insulin secretion pathway[52]. As the bursa site oxygen levels measurements reflect on average an 11% reduction in pO_2 levels compared to the pancreas, the bursa site oxygen levels may be sufficient to support encapsulated endocrine graft function for as long as the microsphere surface remains devoid of fibrotic overgrowth to ensure free nutritional exchange.

Z1-Y15 spheres containing allogeneic islets in NHP

We sought to investigate the potential of the improved sphere formulation, and the improved transplantation methods to support allogeneic islets without immune suppression in NHP. Pancreatic islets were isolated from cynomolgus macaques, encapsulated within Z1-Y15 modified alginate spheres at the 1.5 mm size, and transplanted into the bursa omentalis of non-diabetic cynomolgus monkeys (Supplementary Table 4). Non-diabetic NHP were

Author Manuscript Author Manuscript Author Manuscript Author Manuscript

chosen to remove any potential for hyperglycemia induced glucotoxicity on islet viability and the differences in metabolic profiles between NHP and human species[53–56]. Diabetic NHP require roughly 4 times as much exogenous insulin compared to humans in order to maintain blood glucose homeostasis (NHP: 2–3 UI/kg per day; UIC islet transplant patients: 0.5–0.7 UI/kg per day)[57,58]. NHP islets also have been shown to secrete higher amounts of insulin during *in vitro* glucose challenges compared to human islets and may be related to the higher insulin requirements of the species[56]. These species related metabolic differences may make any information concerning factors such as the optimal number of islets per sphere, curative dose of islets/spheres, or longevity of encapsulated islet graft function difficult to compare between NHP and humans. For these reasons and as a proof of concept, Z1-Y15 spheres containing allogeneic islets were retrieved 1 month and 4 months post transplantation into the bursa omentalis of non-diabetic NHP to assess the biocompatibility of the spheres (PFO) and the presence of viable endocrine tissue.

After 1 month and 4 months post-transplantation, the Z1-Y15 spheres with encapsulated islets were translucent and well distributed within the bursa site (Fig. 2b; Supplementary Fig. 3; Supplementary Video 2). Spheres with encapsulated islets easily dissociated from excised omental tissue and were free of PFO as shown by inverted phase contrast images (Fig. 3a; Supplementary Fig. 4). This is in contrast to control empty SLG20 alginate spheres with substantially more cellular overgrowth. Cells on the surface of the retrieved spheres were dissociated and analyzed using flow cytometry for $CD68^+/CD11b^+$ macrophages: the predominant mediator of foreign body responses to implantable materials[21]. Z1-Y15 spheres with encapsulated islets showed decreased macrophage cellular attachment compared to SLG20 empty alginate spheres (Fig. 3b; Supplementary Fig. 5). For comparison, SLG20 spheres with encapsulated allogeneic islets were also transplanted into the bursa omentalis site. No free spheres could be retrieved from the excised omental tissue as the spheres were surrounded in fibrotic tissue after 1 month (Supplementary Fig. 6). PFO was quantified, and Z1-Y15 spheres with encapsulated islets were substantially less fibrosed than the retrieved SLG20 spheres with encapsulated islets (Fig. 3c; Supplementary Table 5). PFO scores were further reduced when Z1-Y15 spheres were transplanted into the bursa omentalis site compared to the general IP space, which may be indicative of a reduction in material fibrosis by limiting sphere clumping (Supplementary Table 1; Supplementary Table 5). Interestingly, cynomolgus islets encapsulated in SLG20 spheres resulted in fibrosis 1 month post allogeneic transplantation in NHP, but the same SLG20 formulated spheres with cynomolgus islets enabled long-term glycemic control in immune-competent C57BL/6J mice as a xenogeneic transplant model (Supplementary Fig. 7a/b). The encapsulated islets demonstrated marginal fibrosis when retrieved from the IP space of the mice after 1 year (Supplementary Fig. 7c). This further highlights the disconnect between NHP and the most predictive mouse model (C57BL/6J) for testing islet cell encapsulation technologies.

The Z1-Y15 formulation was found to provide long-term protection of viable allogeneic tissue in NHP (Fig. 3d-g). Viability assessments were performed on the encapsulated islets to estimate the number of live cells within the whole islet cell clusters. This method of viability assessment is employed in clinical islet transplantation where gross islet lot viability must be over 75% in order to be deemed suitable for intraportal islet transplantation in the National Institute of Health (NIH) sponsored clinical trial by the Clinical Islet

Author Manuscript Author Manuscript Author Manuscript Author Manuscript

Transplantation consortium[58,59]. Islet viability scores were determined pre-encapsulation (naked), post-encapsulation (pretx), and post retrieval at 1 month and 4 months (Fig. 3d). The viability scores of the islets at each of the time points were then analyzed using the Wilcoxon signed rank test to assess whether median viability was significantly different from 75%. Six out of seven encapsulated islet preparations demonstrated significantly higher viability than 75% from pre-encapsulation (naked), post-encapsulation (pretx), to post retrieval from NHP (Supplementary Table 6). Encapsulated islets from one primate (CN8800) were retrieved at 4 months and presented with PFO and non-viable islets. At the time of transplantation, this same lot of encapsulated islets was also transplanted into a separate primate (CN8801) that yielded viable islets without PFO when retrieved at 4 months. These distinct results using the same lot of material/islets lead us to hypothesize that the cause of PFO formation in the one primate may be related to undocumented differences in the transplant procedure or natural animal variability when using non-inbred NHP models.

The retrieved Z1-Y15 encapsulated islets also demonstrated conservation of functional endocrine tissue (Fig. 3e-g). The islets stained densely for dithizone at both 1 month and 4 months post-transplantation (Fig. 3e). Dithizone is a stain that binds zinc ions within mature insulin granules and is employed during islet isolation to discern endocrine tissue from non-beta cell tissue. The hallmark phenotype of beta cells is an ability to detect glucose changes in extracellular solutions and secrete insulin. This functional capacity of the retrieved encapsulated islets was tested using both static and dynamic glucose challenge assays.

Firstly, glucose stimulated insulin secretion (GSIS) of the encapsulated islets was measured where islets were statically incubated in a low (2 mM) and high (18 mM) glucose solution for 1 hour, and the amount of insulin secreted into the supernatant was quantified. The Z1-Y15 encapsulated allogeneic islets secreted statistically higher levels of insulin under high glucose compared to low glucose at both 1 and 4 months retrievals (Fig. 3f). The glycemic induced stimulation index was lower at 4-months when compared to 1-month; however, this may be related to a less than optimal preparation of islets and a smaller numbers of primates tested at 4-months.

Secondly, intracellular coupling factors that are important mediators in the insulin secretion pathway were measured using a dynamic microfluidic based perifusion glucose challenge assay[52,60]. In beta-cells, glucose-induced insulin secretion is a complex process involving glucose metabolism, mitochondrial energy production, closing of ATP-dependent potassium ion channels, opening of voltage-dependent calcium ion channels (VDCCs), calcium influx, and insulin granule fusion with the cell membrane for insulin secretion, which has a biphasic and oscillatory kinetic pattern[61]. By loading islets with the fluorescent dyes (Rh123, Fura-2), beta cell activity was dynamically assessed to probe mitochondrial activity and membrane ion channel performance after stimulation with high glucose. Retrieved encapsulated islets demonstrated similar mitochondrial membrane potential changes ($\Delta\Psi_m$) and calcium influx $[Ca^{2+}]_i$ levels after stimulation with high glucose (18 mM) compared to encapsulated islets tested pre-transplantation (Fig. 3g). These responses of the retrieved encapsulated islets are indicative of proper mitochondrial energy production and functional

Author Manuscript Author Manuscript Author Manuscript Author Manuscript

VDCCs, which suggest that the intracellular machinery important for insulin secretion are conserved within the retrieved encapsulated islets.

In previous studies, it was suggested that the chemical modification of alginate spheres using triazole ring containing small molecules confers a distinct surface that reduces macrophage activation[26]. This effect did not appear to be directly correlated to bulk sphere physical properties for the sphere formulations tested such as young's modulus, permeability, surface roughness, or protein adsorption[26]. It was previously shown that the adherence of $CD68^+$/$CD11b^+$ positive macrophages correlates with a significant foreign body response and fibrosis of alginate spheres[21]. The adherence of this cell subtype to Z1-Y15 empty spheres was significantly reduced compared to control unmodified alginate formulations[26], and we now show a similar reduction in this immune cell population even with the presence of allogeneic cells in NHP (Fig. 3b). Activated macrophages are known to recruit myofibroblasts (SMA^+), which deposit ECM proteins (collagen I/III, laminin, fibrinogen) in conjunction with macrophages to form the nutrient restrictive matrix[32,62–65]. We hypothesize that the Z1-Y15 chemical modification specifically modulates macrophage activation upstream, which in turn significantly reduces the recruitment of myofibroblasts: the major contributor to downstream fibrosis. The molecular interactions that lead to this macrophage modulation remain unclear but are actively being investigated in our lab.

Through the combination of an anti-fibrotic Z1-Y15 encapsulation material and an alternative transplantation technique into the bursa omentalis, long term protection of viable and glucose responsive allogeneic islets was achieved in NHP without any immunosuppression. This approach can similarly be used for a broad spectrum of applications including localized drug delivery and allogeneic cell-based protein therapies to better manage protein deficiency diseases such as Parkinson's disease, hemophilia, and lysosomal storage disorders. Importantly, considering that clinical trials conducted with encapsulated cadaveric islets were shown to be safe and well tolerated, we believe a similar evaluation in patients using these materials and transplantation methods is warranted, and may provide therapeutic benefit to a select group of diabetic patients with severe hypoglycemic unawareness.

Methods:

Laparoscopic implantation and retrieval of empty alginate spheres formulations from the general IP space of NHP: A-PLO-A, UPMVG-Ba^{2+}, UPMVG-Ca^{2+}/Ba^{2+}, SLG20-Ba^{2+}, Z1-Y19-Ba^{2+}, Z2-Y12-Ba^{2+}, Z1-Y15-Ba^{2+}

All transplant procedures involving both NHP and mice were compliant with the relevant ethical regulations including the guidelines of the National Institute of Health and all procedures were approved in protocols by the animal care committee at UIC. Each of the sphere formulations used in the human clinical trials (A-PLO-A, UPMVG-Ba^{2+}, UPMVG-Ca^{2+}/Ba^{2+}) were produced using methods previously reported[12–15]. The spheres were either produced at each respective institution and shipped to UIC or produced by the original inventor team under cGMP conditions at UIC for implantation into non-diabetic NHP. The control alginate SLG20-Ba^{2+} and the chemically modified alginate derivative spheres (Z1-Y19-Ba^{2+}, Z2-Y12-Ba^{2+}, Z1-Y15-Ba^{2+}) were produced at MIT using methods previously

Author Manuscript Author Manuscript Author Manuscript Author Manuscript

reported[26] and shipped for implantation into non-diabetic NHP. The spheres were implanted laparoscopically and evenly distributed around lobes of the liver in the general IP space of the abdominal cavity, as previously described[17]. The empty plain alginate spheres were retrieved laparoscopically using saline lavages to flush free spheres after 7 days and 1 month post-implantation. The SLG20 Alginate- Ba^{2+} and chemically modified alginate derivative spheres were retrieved using the same laparoscopic procedure after 2 weeks, 1 month, and 6 months post-implantation. The retrieved spheres were then assessed for fibrosis and processed for histological analysis. Omental tissue biopsies containing spheres were also processed for histological analysis.

Z1-Y15 small molecule synthesis

To synthesize the Z1-Y15 small molecule, 4-propargylthiomorpholine 1,1-dioxide (1 eq.) was added to a round bottom flask and dissolved in a methanol:water (5:1) mixture. Then Tris[(1-benzyl-1H-1,2,3-triazol-4-yl)methyl]amine (0.25 eq.), triethylamine (0.25 eq.), and Copper(I) iodide (0.1 eq.) was added. The mixture was purged with nitrogen for 5 min and cooled to 0°C. Then 11-azido-3,6,9-trioxaundecan-1-amine (6.30 g, 28.86 mmol, 1 eq.) was added. The mixture was stirred at room temperature for 5 min and subsequently heated to 55 °C overnight. The reaction mixture was let to cool to room temperature and filtered with a Buchner funnel through 413 filter paper to filter off any insoluble material. The filtrate was washed three times with 50 mL methanol and the solvent was removed under reduced pressure. The crude material was purified via liquid chromatography and characterized with NMR and high-resolution mass spectroscopy.

1H (400 MHz; CDCl3): 2.87 (2H, s, NH2-CH2-CH2-O), 3.05 (8H, m, N-CH2-CH2-S), 3.51 (2H, t, J=5.2Hz, NH2-CH2),3.61 (8H, m, PEG) 3.81 (2H, s, Thiomorpholine-CH2-Triazole), 3.89 (2H, t, J=5.2Hz, N-CH2-CH2-O), 4.55 (t, 2H, J=5.2, N-CH2-CH2-O), 7.69 (1H, s, triazole)

13C (400 MHz; CDCl3): 41.74 (NH2-CH2), 50.42 (N-CH2), 50.56 (N-CH2 Thiomorpholine) 51.52 (S-CH2 Thiomorpholine) 52.2 (Thiomorpholine-CH2-Triazole), 69.54–73.14 (m, PEG), 124.10 (CH triazole), 143.32 (C triazole)

High resolution MS: M+1 = 392.1939

Z1-Y15 alginate synthesis:

In a round bottom flask, 2g of UP-VLVG (1 eq.) (NovaMatrix, Sandvika, Norway) was dissolved in water (70 mL). Once the alginate dissolved, 2-chloro-4,6-dimethoxy-1,3,5-triazine (895.42 mg, 5.10 mmol, 0.5 eq.) and N-methylmorpholine (1.03 g, 10.20 mmol, 1.12 mL, 1 eq.) was added to the solution. Z1-Y15 small molecule (3.99 g, 10.20 mmol, 1 eq.) was weighed in a vial, dissolved in acetonitrile (35 mL) and added to the reaction mixture. The reaction was heated to 55 °C and stirred overnight. The solvents were removed under reduced pressure and 100 mL of Mili Q water was added to re-dissolve the alginate.

The solution was filtered through a 1 cm pad of cyano-silica gel and the filtered solution was dialyzed in a 40 cm long 3.5 K pretreated RC tubing 45 mm X 29 mm in a 4 L beaker. The

Author Manuscript Author Manuscript Author Manuscript Author Manuscript

water was changed after 3 hours, after dialysis overnight, and again after 4 hours. The dialyzed solution was frozen and lyophilized until dry.

NHP pancreatectomy

The donor pancreas procurement was performed under general anesthesia. Using a midline incision both splenorenal and splenocolic ligaments were divided to mobilize the spleen and pancreatic tail. The head of the pancreas and second portion of the duodenum were mobilized using a Kocher maneuver. The lesser sac was opened and dissected exposing the superior mesenteric artery and supraceliac aorta and infra renal aorta. After administration of heparin (200 units/kg), the aorta was cannulated just above its bifurcation using 14GA 1.88IN (BD Angiocath™, NJ, USA). Both supraceliac aorta and inferior mesenteric artery were ligated and the animal was exsanguinated. Cold saline slush was immediately placed into the lesser sac surrounding the body of the pancreas. The pancreas was flushed with 600–800 mL of cold UW solution. The body and neck of the pancreas were carefully excised. The duodenum was carefully separated off the pancreatic head to identify and cannulate the pancreatic duct using a 24G 0.75IN winged cannula (BD Insyte™ Autoguard™ Winged, NJ, USA).

NHP islet isolation

Cynomolgus monkey islets were isolated from donors using a method previously reported[57]. Briefly, the pancreas was perfused with 10–15 mL of enzyme solution (Collagenase Type V; 3.3 mg/mL in cold HBSS) (Sigma-Aldrich, MO, USA) and cut into 8–10 small pieces. The pancreatic tissue was digested in a 125-mL glass Erlenmeyer flask in a 37 °C water bath under gentle agitation for 12–15 minutes. At 10 minutes, the first tissue sample was taken from the flask using a sterile transfer pipette to assess the size of the dissociated tissue and the percentage of free islets. Samples were assessed with dithizone staining under bright-field microscopy until the pancreatic tissue was evenly broken down, and 80 % or more of the islets were free without obvious fragmentation. At this point, the digestion process was quenched by diluting the enzyme/tissue solution with 500 mL of cold HBSS containing 10 % FBS. The tissue was washed 3 times with the cold HBSS solution by centrifugation (200g for 1 minute). The digested tissue was then purified using a discontinuous ficoll density gradient (density: 1.108 g/mL, 1.196 g/mL, and 1.069 g/mL) (Mediatech, Manassas, VA, USA). Based on the volume, the tissue was divided into 50 mL conical tubes (0.5 mL tissue concentration for each tube). The centrifuge speed for purification was 640g for 15 minutes. The islet interface between density of 1.196 and 1.069 was aspirated manually and washed 3 times with CMRL Supplemented culture medium containing 10 % FBS, 0.2 % ciprofloxacin, and 0.1 % insulin transferrin-selenium. The purified islets were then cultured overnight at 37 °C and 5 % CO_2.

NHP islets encapsulation within Z1-Y15 alginate

The encapsulation of cynomolgus monkey islets within Z1-Y15 alginate was performed at UIC in conjunction with researchers from MIT according to methods previously reported[26]. Prior to encapsulation, all buffers were sterilized by autoclave and alginate solutions were sterile filtered through a 0.2 μm filter. All experimental procedures were conducted in a biosafety cabinet. Cynomolgus monkey islets were collected and washed twice with a

Author Manuscript Author Manuscript Author Manuscript Author Manuscript

calcium-free Krebs-Henseleit solution (4.7 mM KCl, 25 mM HEPES, 1.2 mM KH_2PO_4, 1.2 mM $MgSO_4 \times 7H_2O$, 135 mM NaCl, pH ≈ 7.4, ≈290 mOsm) by centrifugation at 200*g* for 1 min at room temperature. After the final wash, the entire supernatant was carefully removed, leaving an islet pellet with little residual liquid. Sterile cotton swabs were then used to remove any residual washing solution on the sides of the conical tube, which would dilute the alginate solution.

The Z1-Y15 conjugated UP-VLVG alginate was initially dissolved at 5 % wt/v in 0.8 % saline overnight. This was then blended overnight with a 3 % wt/v SLG100 (also dissolved in 0.8% saline) at a volume ratio of 70 % Z1-Y15-VLVG alginate to 30 % SLG100. 5 mL of the final Z1-Y15 working alginate solution was added to the islet pellet at an islet seeding density of 1,000 islets per 1 mL Z1-Y15 alginate solution. The mixture was gently agitated to uniformly disperse the islets within the Z1-Y15 alginate solution and transferred to a 5 mL syringe with an 18G blunt tipped needle (SAI Infusion Technologies, IL, USA). An electrostatic droplet generator was set up in the biosafety cabinet as follows: an ES series 0–100-kV, 20-watt high-voltage power generator (Gamma ES series, Gamma High-Voltage Research, FL, USA) was connected to the blunt-tipped needle. A glass dish containing a 20 mM barium and 5% mannitol solution (Sigma-Aldrich, MO, USA) was then grounded via metal forceps. A syringe pump (Pump 11 Pico Plus, Harvard Apparatus, MA, USA) was oriented vertically and used to extrude alginate droplets into the gelation solution over a period of 20 minutes and gelled for an additional 5 minutes. The settings of the PicoPlus syringe pump were 12.06 mm diameter and 0.18 mL/min flow rate. After the spheres were formed, they were collected and washed with HEPES buffer (NaCl 15.428 g, KCl 0.70 g, $MgCl_2 \cdot 6H_2O$ 0.488 g, 50 mL of HEPES (1 M) buffer solution (Gibco, Life Technologies, California, USA) in 2 liters of deionized water) four times. The spheres were then washed two times in 0.8 % saline and two more times with culture media, CMRL1066 Supplemented (Mediatech Inc., Herndon, VA) containing 0.2 % Cipro, 10 % Fetal bovine serum, and 0.1 % Insulin Transferrin Selenium (ITS 100×) (Gibco, Life Technologies, California, USA). The Z1-Y15 spheres with encapsulated islets were then cultured for 2 days prior to transplantation in NHP.

Bursa Omentalis laparoscopic transplantation of encapsulated islets

Under general anesthesia, a small supra umbilical midline incision was performed to place a 8 mm trocar (ENDOPATH® XCEL™ ETHICON ENDO-SURGERY®, Somerville, NJ, USA). The camera was introduced to confirm the trocar location. Pneumoperitoneum was created with CO_2 at a pressure of 10–14 mmHg, and two additional small incisions were performed on the left and right flank and 5 mm trocars were inserted into peritoneal cavity. An endoscopic grasping forceps (Endo Dissect™ COVIDIEN™, Somerville, NJ, USA) and endoscopic scissors (Endo Shears™ COVIDIEN™, Somerville, NJ, USA) were inserted into each of the two trocars. The stomach was gently lifted using the laparoscopic grasper and a small incision was made into an avascular portion of the gastrocolic ligament (anterior layer of the greater omentum below the greater curvature of the stomach and above the transverse colon). A 2 mL pipette was connected by silicone tubing to a 60 mL lavage syringe containing the spheres. The pipette was then placed into the lesser sac and the spheres were gently infused. Once the spheres had been infused into the bursa omentalis, the

Author Manuscript Author Manuscript Author Manuscript Author Manuscript

stomach was gently lowered to seal the opening. The trocars were removed and the three small incisions were closed in two layers using 3–0 Vicryl (ETHICON®, Somerville, NJ, USA) for the muscle and for 5–0 Vicryl (ETHICON®, Somerville, NJ, USA) for the skin (subcuticular). Bupivicaine was infused along the incision line to reduce postoperative pain.

Retrieval of encapsulated cynomolgus monkey islets

Under general anesthesia and using the previously described laparoscopic technique, 20–30 mL of normal saline was used as a lavage to flush free spheres from the intraperitoneal space. Free spheres in the lavage solution in the general IP space were then aspirated and collected for analysis. For spheres transplanted into the bursa omentalis, the greater omentum was pulled through the laparoscopic camera port incision to exam the sphere laminar distributions. The greater omentum containing spheres was then resected and agitated with saline in a surgical bowl to dissociate spheres from the greater omentum. In the case no free spheres were found in the lavage solutions or from the agitated greater omentum resections, biopsies of omental tissue containing spheres were removed for histological analysis.

Inverted phase contrast imaging

For phase-contrast imaging, retrieved materials were gently washed twice with Krebs buffer and transferred into 35 mm Petri dishes for phase-contrast microscopy using an Evos Xl microscope (Advanced Microscopy Group). Images were then converted to black and white, and colors inverted using ImageJ software. The colors were inverted in order to see the sphere outline as well as the presence of islets within the spheres. Original images are shown in the top right corner of each inverted phase contrast image. For bright-field imaging of retrieved materials, samples were gently washed using Krebs buffer and transferred into 35 mm Petri dishes for bright-field imaging using a Leica stereoscopic microscope.

Fibrosis scoring of retrieved spheres

The retrieved spheres were assessed under a bright-field microscope for the degree of fibrotic overgrowth using a method previously reported[66]. The degree of fibrotic overgrowth was determined by categorizing the retrieved spheres for the percentage of the sphere surface area that was covered by overgrowth: 0 <25%, 25–50%, 50–75%, 75–100%. Data is presented as the percentage of spheres assessed in each category for each primate. The total number of spheres assessed per primate retrieval is provided in supplementary information.

Flow cytometry analysis of cells dissociated from retrieved spheres

Single-cell suspensions of cells from the surfaces of freshly retrieved spheres were prepared using a gentleMACS Dissociator (Miltenyi Biotec, Auburn, CA) according to the manufacturer's protocol. Single-cell suspensions were prepared in PEB dissociation buffer (1× PBS, pH 7.2, 0.5% BSA, and 2 mM EDTA) and suspensions were passed through 70 μm filters (Cat. #22363548, Fisher Scientific, Pittsburgh, PA). Single-cell populations were then subjected to red blood cell lysis with 5 mL of 1× RBC lysis buffer (Cat. #00–4333, eBioscience, San Diego, CA, USA) for 5 min at 4 °C. The reaction was terminated by the addition of 20 mL of sterile 1× PBS. The remaining cells were centrifuged at 300–400*g* at

Author Manuscript Author Manuscript Author Manuscript Author Manuscript

4 °C and resuspended in a minimal volume (~50 μL) of eBioscience Staining Buffer (cat. #00–4222) for antibody incubation. All samples were then co-stained in the dark for 25 min at 4 °C with two of the fluorescently tagged monoclonal antibodies specific for the cell markers CD68 (1 μL (0.5 μg) per sample; CD68-Alexa647, Clone KPI, Cat. no. sc-20060, Santa Cruz Biotechnology) and CD11b (1 μL (0.2 μg) per sample; CD11b-Alexa-488, Clone M1/70, Cat. #101217, BioLegend). 2 mL of eBioscience Flow Cytometry Staining Buffer (cat. #00–4222, eBioscience) was then added, and the samples were centrifuged at 400–500*g* for 5 min at 4 °C. Supernatants were removed by aspiration, and this wash step was repeated two more times with staining buffer. Following the third wash, each sample was resuspended in 500 μL of Flow Cytometry Staining Buffer and run through a 40 μm filter (Cat. #22363547, Fisher Scientific) for eventual analysis using a BD FACSCalibur (cat. #342975), BD Biosciences, San Jose, CA, USA). For proper background and laser intensity settings, unstained, single antibody, and IgG (labeled with either Alexa-488 (CA# 400625, BioLegend) or Alexa-647 (CA# 400526, BioLegend) controls were also run.

Histology of retrieved freely floating spheres

Post retrieval, freely floating spheres were rinsed three times with PBS and fixed in 10 % formalin overnight. After fixation, the spheres were rinsed twice with PBS, and dehydrated in gradually ascending ethanol solutions for 20 min each. The spheres were cleared in xylene for 10 min, and incubated in a 50/50 solution of xylene and paraffin overnight at 57 °C. On day 3, the spheres were transferred to paraffin twice for 1 hr. each, and then embedded in a paraffin mold. Subsequently, embedded spheres were sectioned at 5 μm thickness onto positively charged lysine microscope slides. Tissue sections were then stained for hematoxylin and eosin (H&E) to assess pericapsular cellular overgrowth.

Histology of omental biopsies containing spheres

Biopsies containing embedded spheres were fixed in 10 % formalin overnight, rinsed twice with PBS and stored overnight in 70% EtOH. Biopsies were further dehydrated the next day in ascending EtOH solutions, cleared in xylene and embedded in a paraffin block. Subsequently, embedded biopsies were sectioned at 5 μm thickness and stained for H&E to assess tissue overgrowth of the spheres. If morphological observation of H&E stained tissue sections showed multi-layer cellular overgrowth of the spheres, immunohistochemistry (IHC) was performed on the adjacent tissue sections to investigate the cellular populations involved in the PFO. Sections were immunofluorescently labeled for $CD11b^+$ myeloid cells and alpha-smooth muscle actin positive (α-SMA^+) myofibroblasts. Slide sections were deparaffinized and rehydrated tissue sections were immersed in citrate buffer at pH 6 to perform the heat-induced epitope retrieval (HIER). Tissue sections were then rinsed with Tris-buffered saline (TBS) plus 0.025% triton X-100 and blocked with goat normal serum for 1 hr at room temperature. Primary antibodies mouse IgG1 against CD11b (1:100 clone ICRF44; Cat#: ab34216, Abcam, Cambridge, MA, USA), and α-SMA (1:100 clone IA4; Cat # ab7817; Abcam, Cambridge, MA, USA), were applied on serial sections and incubated overnight at 4 ºC. After rinsing with TBS plus 0.025 % triton X-100, fluorescently labeled secondary antibodies Alexa Fluor 594 anti-mouse (1:200; Cat# A-11032; Invitrogen, Grand Island, NY, USA) were applied and incubated for 1 hr at room temperature. DAPI nuclear counterstain was then applied and the coverslips mounted. All stained tissue sections

Author Manuscript Author Manuscript Author Manuscript Author Manuscript

were viewed under a Leica DM 200 microscope and images captured with QICAM Fast1394 digital camera and processed with Qcapture Pro5.1 program.

Partial oxygen pressure (pO_2) measurements of various transplantation sites in NHP

Monkeys were sedated and anaesthetized in accordance with approved animal protocols at the University of Illinois at Chicago. The animals were ventilated with room air to mainain physiological arterial pO_2. This was determined by measuring the partial pressure of oxygen (pO_2, mm/Hg)), total Hemoglobin (tHb, g/dL) and O_2 saturation (SO_2, %) of NHP before intubation (while sedated but breathing normal air) and post intubation with different fractions of inspired oxygen (FiO_2). A left femoral arterial line was set to facilitate repeated blood draws (1 mL) from the cynomolgus monkey. Following the pre-intubation blood draw, the animal was intubated and placed on a different fractions of inspired oxygen (FiO_2) (50 % − 21 %) for three minutes. Blood samples were collected from the arterial line and placed in a Blood Gas Analyzer cassette. Arterial pO_2, tHb, and SO_2 were analyzed using the IDEXX VetStat Electrolyte and Blood Gas Analyzer.

For pO2 measurements of transplantation sites in NHP, no CO_2 pneumoperitoneum was used. A miniaturized Clark type oxygen probe (Unisense, Denmark) was used to determine pO_2 inside the abdominal cavity. The working principle of the oxygen sensor is based on diffusion of oxygen through a silicone membrane to an oxygen-reducing cathode. The reducing cathode is polarized against an internal Ag/AgCI anode. This microscale sensor (2–3 μm) can produce a minute current which is directly proportional to the oxygen tension in the tissue to which it is applied at high spatial resolution and at a fast response time less than 0.3 s. In the animals tested, three pO_2 measurements were taken from each site. For intraperitoneal space, intramuscular and subcutaneous a 18 G needle was inserted into the site followed by the insertion of the probe. For the organ sites the probe was placed into close proximity to the kidney, liver or pancreas. At each site the probe was placed for 3–5 minutes prior to taking measurements.

Dithizone staining

Dithizone was prepared by mixing 100 mg of dithizone in 10 mL DMSO and 40 mL HBSS (Sigma, St. Louis, MO, USA) and filtering through a 0.22 μm filter. Encapsulated monkey islets were placed in a 50 mL tube and 5 mL of dithizone was added and incubated for 3 minutes. The encapsulated islets were then quickly washed 3 times with 10 mL HBSS, followed by two 5 min incubations in fresh 10 mL HBSS to reduce background. The encapsulated islets were then placed in a 100 mm Petri dish and imaged using a bright-field microscope.

Islet viability

Cell viability of cynomolgus monkey islets was assessed post isolation, post encapsulation and post retrieval by dual fluorescence staining with inclusion/exclusion dyes fluorescein diacetate (FDA) (Sigma, St. Louis, MO, USA) for live cells and propidium iodide (PI) (Sigma, St. Louis, MO, USA) for dead cells. Briefly, naked or encapsulated islets were rinsed twice with 10 mL HBSS (Mediatech Inc., Herndon, VA, USA) and then mixed with 2 mL of 0.46 μM FDA and 14.34 μM PI in HBSS. A fluorescent microscope with filters for

Author Manuscript Author Manuscript Author Manuscript Author Manuscript

FDA (excitation wavelength 488 nm, emission wavelength 520 nm) and PI (excitation wavelength 534 nm, emission wavelength 617 nm) was used to assess the viability of the islets. Percentages of total viable cells within 25–50 whole islets were estimated by a single operator trained in islet isolation protocols approved by the NIH funded clinical trial by the Clinical Islet Transplantation consortium[58,59].

Glucose stimulated insulin secretion (GSIS)

GSIS was performed on encapsulated cynomolgus monkey islets post retrieval from NHP. Encapsulated islets were collected in a 50 mL conical tube and quickly washed 3× with 25 mL saline. 25 mL of Krebs-Ringer buffer containing 2 mM glucose (KR2) was then added to the encapsulated islets and the samples were incubated for 10 min. This wash step was repeated 3×. Encapsulated islets were then placed into a Petri dish containing 20 mL of fresh KR2. 10 encapsulated islets were then handpicked under bright-field microscopy and placed into 12 μm porous PET membrane sieves (Merck Millipore, MA, USA). Sieves containing islets were then transferred into 1 mL KR2 solution for 30 min (Pre-wash). The sieves were then transferred into fresh 1 mL KR2 solution for 1 hour (Wash). The sieves were transferred to 1 mL fresh 1 mL KR2 solution for 1 hour (Low). The sieves were then transferred into 1 mL Krebs-Ringer buffer containing 18 mM glucose (High) for 1 hour. Supernatants were then collected from the low (KR2) and high (KR18) wells and the insulin concentrations were quantified by human insulin ELISA (ALPCO, NH, USA) in duplicates without sample dilution.

Real-time fluorescence imaging of islet intracellular calcium and mitochondrial potential changes in response to dynamic glucose challenge

Real-time fluorescence imaging of islet intracellular calcium $[Ca^{2+}]_i$ was performed in a microfluidic device modified for encapsulated islets[60]. In brief, encapsulated cynomolgus monkey islets were incubated with 5 μM Fura-2/AM (Thermo Fisher Scientific, USA) at 37 °C in Krebs-Ringer buffer (KRB) supplemented with 2 mM glucose (KRB2) and 0.5% BSA for 35 min. The microfluidic device was then primed and placed on an inverted epifluorescence microscope (Leica DMI 4000B, IL, USA). Excess dye was washed out with KRB2 for 35 min at a rate of 500 μL/min. Dual-wavelength Fura-2/AM dye were excited ratiometrically at 340 and 380 nm. The changes in the $[Ca^{2+}]_i$ levels are expressed as F340/F380 (% increase from basal 2 mM glucose). Excitation wavelengths were controlled by excitation filters (Chroma Technology, VT, USA) mounted in a Lambda DG-4 wavelength switcher. Emission of Fura-2/AM was filtered using a Fura2/FITC polychroic beam splitter and a double band emission filter (510 nm, 530 nm) (Chroma Technology. Part number: 73.100bs). HCImage software (Hamamatsu Corp, IL, USA) was used for imaging acquisition and analysis. Images were collected with a high-speed, high-resolution charge coupled camera (CCD, ORCA-R2 with ER chip 1344X1024, Hamamatsu, Inc.).

Individual islet intracellular calcium responses were assessed with the following perifusion protocol: KRB2 (5 min), 18 mM glucose (20 min). The area under the curve for the time period of stimulation was calculated for each individual islet in order to statistically compare groups using one-way ANOVA ($p < 0.05$ as significant).

Author Manuscript Author Manuscript Author Manuscript Author Manuscript

Statistical analysis:

Data are expressed as box and whisker plots with median, upper and lower quartile ranges, outliers, and 1.5× IQR, unless specified otherwise. $n = 7$ for non-human primates transplanted with Z1-Y15 encapsulated allogeneic islets; other primate numbers per treatment group are otherwise specified. Flow cytometry data were analyzed for statistical significance by one-way ANOVA with Bonferroni multiple comparison correction. Partial oxygen pressures (pO_2) of various transplantation sites were analyzed for statistical significance by one-way ANOVA and multiple comparisons using Fisher's LSD. Viability scores are presented as individual islets assessed at each time point from NHP experiments with non-fibrosed spheres. Median viability is depicted due to non-normality. Median viabilities were analyzed using the Wilcoxon signed rank test to assess whether median viability was significantly different from 75%, as a biological reference value. Glucose stimulated insulin secretion data were analyzed for statistical significance using the two-tailed Wilcoxon matched-pairs signed-rank test and insulin concentrations from high and low glucose supernatants from the same individual islet samples of Z1-Y15 spheres with encapsulated allogeneic islets. Low and high glucose insulin concentrations from 1 month and 4 months retrieved Z1-Y15 spheres with encapsulated islets were compared using the non-parametric unpaired Mann-Whitney test. Intracellular calcium influx and mitochondrial potential changes in response to perifusion glucose challenge were analyzed for statistical significance by one-way analysis of variance (ANOVA) by comparing the average AUC of $[Ca^{2+}]_i$ % of intracellular calcium influx and the average percent decrease in mitochondrial potential changes ($\Delta\Psi_m$ % change) of individual islets in response to 18 mM glucose stimulus. Statistical analyses were performed using GraphPad Prism 5 software (GraphPad Software, Inc); * $p < 0.05$, ** $p < 0.01$, *** $p < 0.001$, and **** $p < 0.0001$.

Supplementary Material

Refer to Web version on PubMed Central for supplementary material.

Acknowledgments

Acknowledgments:

This work was supported jointly by the Chicago Diabetes Project and the JDRF and the Leona M. and Harry B. Helmsley Charitable Trust (grant no. 3-SRA-2014–285-M-R (R.L. and D.G.A.)), the US National Institutes of Health (grants DK091526 (J.O.) EB000244 (R.L.), EB000351 (R.L.), DE013023 (R.L.), CA151884 (R.L.) and UC4DK104218 (D.L.G.)), and through a generous gift from the Tayebati Family Foundation (D.G.A. and R.L.). This work was also supported by the Slovak Research and Development Agency under contract numbers APVV-14–858 (I.L.). O.V. was supported by JDRF and Department of Defense Congressionally Directed Medical Research Program (DOD/CDMRP) postdoctoral fellowships (grant no 3–2013-178 and W81XWH-13–1-0215, respectively). J.C.D. was supported by JDRF postdoctoral fellowship (grant no. 3-PDF-2015–91-A-N). The authors acknowledge Dr. Lisa Halliday and the veterinary staff at the Biological Resource Laboratories at UIC for their assistance and technical support during the course of the studies. We thank Drs. Ricardo Calafiore and Giuseppe Basta from the University of Perugia for kindly producing the A-PLO-A spheres under cGMP conditions at the University of Illinois at Chicago for the herein described experiments. We thank Bernie Tuch and his team at the Diabetes Transplant Unit, Prince of Wales Hospital, Sydney, Australia for the production of the UPMVG-Ba^{2+} spheres and sharing his experience from the clinical trials in encapsulated islet transplant trials conducted in Sydney, Australia. We thank Dr. Hok Hei Tam for his advice on statistical analysis of data sets.

Author Manuscript Author Manuscript Author Manuscript Author Manuscript

References:

1. Chang TM Semipermeable Microcapsules. Science 146, 524–525 (1964). [PubMed: 14190240]
2. Lim F & Sun AM Microencapsulated islets as bioartificial endocrine pancreas. Science 210, 908–910 (1980). [PubMed: 6776628]
3. Strand BL, Coron AE & Skjak-Braek G Current and Future Perspectives on Alginate Encapsulated Pancreatic Islet. Stem Cells Transl Med 6, 1053–1058 (2017). [PubMed: 28186705]
4. Haug A & Smidsrod O Selectivity of Some Anionic Polymers for Divalent Metal Ions. Acta Chem Scand 24, 843-& (1970).
5. Kollmer M, Appel AA, Somo SI & Brey EM Long-Term Function of Alginate-Encapsulated Islets. Tissue Eng Part B Rev (2015).
6. Mooranian A, Negrulj R, Arfuso F & Al-Salami H Characterization of a novel bile acid-based delivery platform for microencapsulated pancreatic beta-cells. Artif Cells Nanomed Biotechnol 44, 194–200 (2016). [PubMed: 25014218]
7. Kleinberger RM, Burke NA, Zhou C & Stover HD Synthetic polycations with controlled charge density and molecular weight as building blocks for biomaterials. J Biomater Sci Polym Ed 27, 351–369 (2016). [PubMed: 26754568]
8. Duvivier-Kali VF, Omer A, Lopez-Avalos MD, O'Neil JJ & Weir GC Survival of microencapsulated adult pig islets in mice in spite of an antibody response. Am J Transplant 4, 1991–2000 (2004). [PubMed: 15575901]
9. Duvivier-Kali VF, Omer A, Parent RJ, O'Neil JJ & Weir GC Complete protection of islets against allorejection and autoimmunity by a simple barium-alginate membrane. Diabetes 50, 1698–1705 (2001). [PubMed: 11473027]
10. Omer A, et al. Long-term normoglycemia in rats receiving transplants with encapsulated islets. Transplantation 79, 52–58 (2005). [PubMed: 15714169]
11. Dolgin E Diabetes: Encapsulating the problem. Nature 540, S60–S62 (2016). [PubMed: 27926697]
12. Basta G, et al. Long-term metabolic and immunological follow-up of nonimmunosuppressed patients with type 1 diabetes treated with microencapsulated islet allografts: four cases. Diabetes Care 34, 2406–2409 (2011). [PubMed: 21926290]
13. Calafiore R, et al. Microencapsulated pancreatic islet allografts into nonimmunosuppressed patients with type 1 diabetes: first two cases. Diabetes Care 29, 137–138 (2006). [PubMed: 16373911]
14. Tuch BE, et al. Safety and viability of microencapsulated human islets transplanted into diabetic humans. Diabetes Care 32, 1887–1889 (2009). [PubMed: 19549731]
15. Jacobs-Tulleneers-Thevissen D, et al. Sustained function of alginate-encapsulated human islet cell implants in the peritoneal cavity of mice leading to a pilot study in a type 1 diabetic patient. Diabetologia 56, 1605–1614 (2013). [PubMed: 23620058]
16. O'Sullivan ES, Vegas A, Anderson DG & Weir GC Islets transplanted in immunoisolation devices: a review of the progress and the challenges that remain. Endocr Rev 32, 827–844 (2011). [PubMed: 21951347]
17. Qi M, et al. A recommended laparoscopic procedure for implantation of microcapsules in the peritoneal cavity of non-human primates. J Surg Res 168, e117–123 (2011). [PubMed: 21435661]
18. de Vos P, Hamel AF & Tatarkiewicz K Considerations for successful transplantation of encapsulated pancreatic islets. Diabetologia 45, 159–173 (2002). [PubMed: 11935147]
19. Vaithilingam V & Tuch BE Islet transplantation and encapsulation: an update on recent developments. Rev Diabet Stud 8, 51–67 (2011). [PubMed: 21720673]
20. Desai T & Shea LD Advances in islet encapsulation technologies. Nat Rev Drug Discov (2016).
21. Doloff JC, et al. Colony stimulating factor-1 receptor is a central component of the foreign body response to biomaterial implants in rodents and non-human primates. Nat Mater (2017).
22. King A, Sandler S & Andersson A The effect of host factors and capsule composition on the cellular overgrowth on implanted alginate capsules. J Biomed Mater Res 57, 374–383 (2001). [PubMed: 11523032]

Author Manuscript Author Manuscript Author Manuscript Author Manuscript

23. Phillips KA, et al. Why primate models matter. Am J Primatol 76, 801–827 (2014). [PubMed: 24723482]
24. Mestas J & Hughes CC Of mice and not men: differences between mouse and human immunology. J Immunol 172, 2731–2738 (2004). [PubMed: 14978070]
25. Messaoudi I, Estep R, Robinson B & Wong SW Nonhuman primate models of human immunology. Antioxid Redox Signal 14, 261–273 (2011). [PubMed: 20524846]
26. Vegas AJ, et al. Combinatorial hydrogel library enables identification of materials that mitigate the foreign body response in primates. Nat Biotechnol 34, 345–352 (2016). [PubMed: 26807527]
27. Veiseh O, et al. Size- and shape-dependent foreign body immune response to materials implanted in rodents and non-human primates. Nat Mater 14, 643–651 (2015). [PubMed: 25985456]
28. Morch YA, Donati I, Strand BL & Skjak-Braek G Effect of Ca2+, Ba2+, and Sr2+ on alginate microbeads. Biomacromolecules 7, 1471–1480 (2006). [PubMed: 16677028]
29. Qi M, et al. Encapsulation of human islets in novel inhomogeneous alginate-ca2+/ba2+ microbeads: in vitro and in vivo function. Artif Cells Blood Substit Immobil Biotechnol 36, 403–420 (2008). [PubMed: 18925451]
30. Morch YA, et al. Binding and leakage of barium in alginate microbeads. J Biomed Mater Res A 100, 2939–2947 (2012). [PubMed: 22700168]
31. Rokstad AM, Lacik I, de Vos P & Strand BL Advances in biocompatibility and physico-chemical characterization of microspheres for cell encapsulation. *Adv Drug* Deliv Rev 67–68, 111–130 (2014).
32. Anderson JM, Rodriguez A & Chang DT Foreign body reaction to biomaterials. Semin Immunol 20, 86–100 (2008). [PubMed: 18162407]
33. Kolb M, et al. Differences in the fibrogenic response after transfer of active transforming growth factor-beta1 gene to lungs of “fibrosis-prone” and “fibrosis-resistant” mouse strains. Am J Respir Cell Mol Biol 27, 141–150 (2002). [PubMed: 12151305]
34. Vegas AJ, et al. Long-term glycemic control using polymer-encapsulated human stem cell-derived beta cells in immune-competent mice. Nat Med 22, 306–311 (2016). [PubMed: 26808346]
35. Towell ME, Lysak I, Layne EC & Bessman SP Tissue oxygen tension in rabbits measured with a galvanic electrode. J Appl Physiol 41, 245–250 (1976). [PubMed: 956108]
36. Klossner J, Kivisaari J & Niinikoski J Oxygen and carbon dioxide tensions in the abdominal cavity and colonic wall of the rabbit. Am J Surg 127, 711–715 (1974). [PubMed: 4832139]
37. Goh F, Long R, Jr., Simpson N & Sambanis A Dual perfluorocarbon method to noninvasively monitor dissolved oxygen concentration in tissue engineered constructs in vitro and in vivo. Biotechnol Prog 27, 1115–1125 (2011). [PubMed: 21608139]
38. Christoffersson G, et al. Clinical and experimental pancreatic islet transplantation to striated muscle: establishment of a vascular system similar to that in native islets. Diabetes 59, 2569–2578 (2010). [PubMed: 20651296]
39. Toso C, et al. Effect of microcapsule composition and short-term immunosuppression on intraportal biocompatibility. Cell Transplant 14, 159–167 (2005). [PubMed: 15881425]
40. Dufrane D, et al. The influence of implantation site on the biocompatibility and survival of alginate encapsulated pig islets in rats. Biomaterials 27, 3201–3208 (2006). [PubMed: 16497373]
41. Veriter S, et al. In vivo selection of biocompatible alginates for islet encapsulation and subcutaneous transplantation. Tissue Eng Part A 16, 1503–1513 (2010). [PubMed: 20001535]
42. Liu XY, Nothias JM, Scavone A, Garfinkel M & Millis JM Biocompatibility investigation of polyethylene glycol and alginate-poly-L-lysine for islet encapsulation. ASAIO J 56, 241–245 (2010). [PubMed: 20400892]
43. Yang KC, et al. Comparison of bioartificial pancreas performance in the bone marrow cavity and intramuscular space. Arch Med Res 41, 151–153 (2010). [PubMed: 20682171]
44. Kobayashi T, et al. Survival of microencapsulated islets at 400 days posttransplantation in the omental pouch of NOD mice. Cell Transplant 15, 359–365 (2006). [PubMed: 16898230]
45. Pareta R, et al. Long-term function of islets encapsulated in a redesigned alginate microcapsule construct in omentum pouches of immune-competent diabetic rats. Pancreas 43, 605–613 (2014). [PubMed: 24681880]

Author Manuscript Author Manuscript Author Manuscript Author Manuscript

46. Robles L, Storrs R, Lamb M, Alexander M & Lakey JR Current status of islet encapsulation. Cell Transplant 23, 1321–1348 (2014). [PubMed: 23880554]
47. Zhu H, et al. Selection of Implantation Sites for Transplantation of Encapsulated Pancreatic Islets. Tissue Eng Part B Rev (2018).
48. Pepper AR, et al. A prevascularized subcutaneous device-less site for islet and cellular transplantation. Nat Biotechnol 33, 518–523 (2015). [PubMed: 25893782]
49. Stokes RA, et al. Transplantation sites for human and murine islets. Diabetologia 60, 1961–1971 (2017). [PubMed: 28735354]
50. Olsson R & Carlsson PO A low-oxygenated subpopulation of pancreatic islets constitutes a functional reserve of endocrine cells. Diabetes 60, 2068–2075 (2011). [PubMed: 21788581]
51. Avgoustiniatos ES & Colton CK Effect of external oxygen mass transfer resistances on viability of immunoisolated tissue. Ann Ny Acad Sci 831, 145–167 (1997). [PubMed: 9616709]
52. Nourmohammadzadeh M, et al. Microfluidic array with integrated oxygenation control for real-time live-cell imaging: effect of hypoxia on physiology of microencapsulated pancreatic islets. Anal Chem 85, 11240–11249 (2013). [PubMed: 24083835]
53. Kim WH, et al. Exposure to chronic high glucose induces beta-cell apoptosis through decreased interaction of glucokinase with mitochondria: downregulation of glucokinase in pancreatic beta-cells. Diabetes 54, 2602–2611 (2005). [PubMed: 16123348]
54. Biarnes M, et al. Beta-cell death and mass in syngeneically transplanted islets exposed to short- and long-term hyperglycemia. Diabetes 51, 66–72 (2002). [PubMed: 11756324]
55. Vallabhajosyula P, et al. Effect of the Diabetic State on Islet Engraftment and Function in a Large Animal Model of Islet-Kidney Transplantation. Cell Transplant 26, 1755–1762 (2017). [PubMed: 29338381]
56. Mueller KR, et al. Differences in glucose-stimulated insulin secretion in vitro of islets from human, nonhuman primate, and porcine origin. Xenotransplantation 20, 75–81 (2013). [PubMed: 23384163]
57. Qi M, et al. Implementation of a simplified method of islet isolation for allogeneic islet transplantation in cynomolgus monkeys. Pancreas 43, 226–235 (2014). [PubMed: 24518500]
58. Qi M, et al. Five-year follow-up of patients with type 1 diabetes transplanted with allogeneic islets: the UIC experience. Acta diabetologica 51, 833–843 (2014). [PubMed: 25034311]
59. Gangemi A, et al. Islet transplantation for brittle type 1 diabetes: the UIC protocol. Am J Transplant 8, 1250–1261 (2008). [PubMed: 18444920]
60. Adewola AF, et al. Microfluidic perifusion and imaging device for multi-parametric islet function assessment. Biomed Microdevices 12, 409–417 (2010). [PubMed: 20300858]
61. Keizer J & Magnus G ATP-sensitive potassium channel and bursting in the pancreatic beta cell. A theoretical study. Biophys J 56, 229–242 (1989). [PubMed: 2673420]
62. Klingberg F, Hinz B & White ES The myofibroblast matrix: implications for tissue repair and fibrosis. J Pathol 229, 298–309 (2013). [PubMed: 22996908]
63. Sheikh Z, Brooks PJ, Barzilay O, Fine N & Glogauer M Macrophages, Foreign Body Giant Cells and Their Response to Implantable Biomaterials. Materials (Basel) 8, 5671–5701 (2015). [PubMed: 28793529]
64. Wynn TA & Vannella KM Macrophages in Tissue Repair, Regeneration, and Fibrosis. Immunity 44, 450–462 (2016). [PubMed: 26982353]
65. Mantovani A, Biswas SK, Galdiero MR, Sica A & Locati M Macrophage plasticity and polarization in tissue repair and remodelling. J Pathol 229, 176–185 (2013). [PubMed: 23096265]
66. Vaithilingam V, et al. Beneficial effects of coating alginate microcapsules with macromolecular heparin conjugates-in vitro and in vivo study. Tissue Eng Part A 20, 324–334 (2014). [PubMed: 23971677]
67. Kayaalp C Bursectomy at radical gastrectomy. World J Gastrointest Surg 7, 249–253 (2015). [PubMed: 26523213]

Author Manuscript Author Manuscript Author Manuscript Author Manuscript

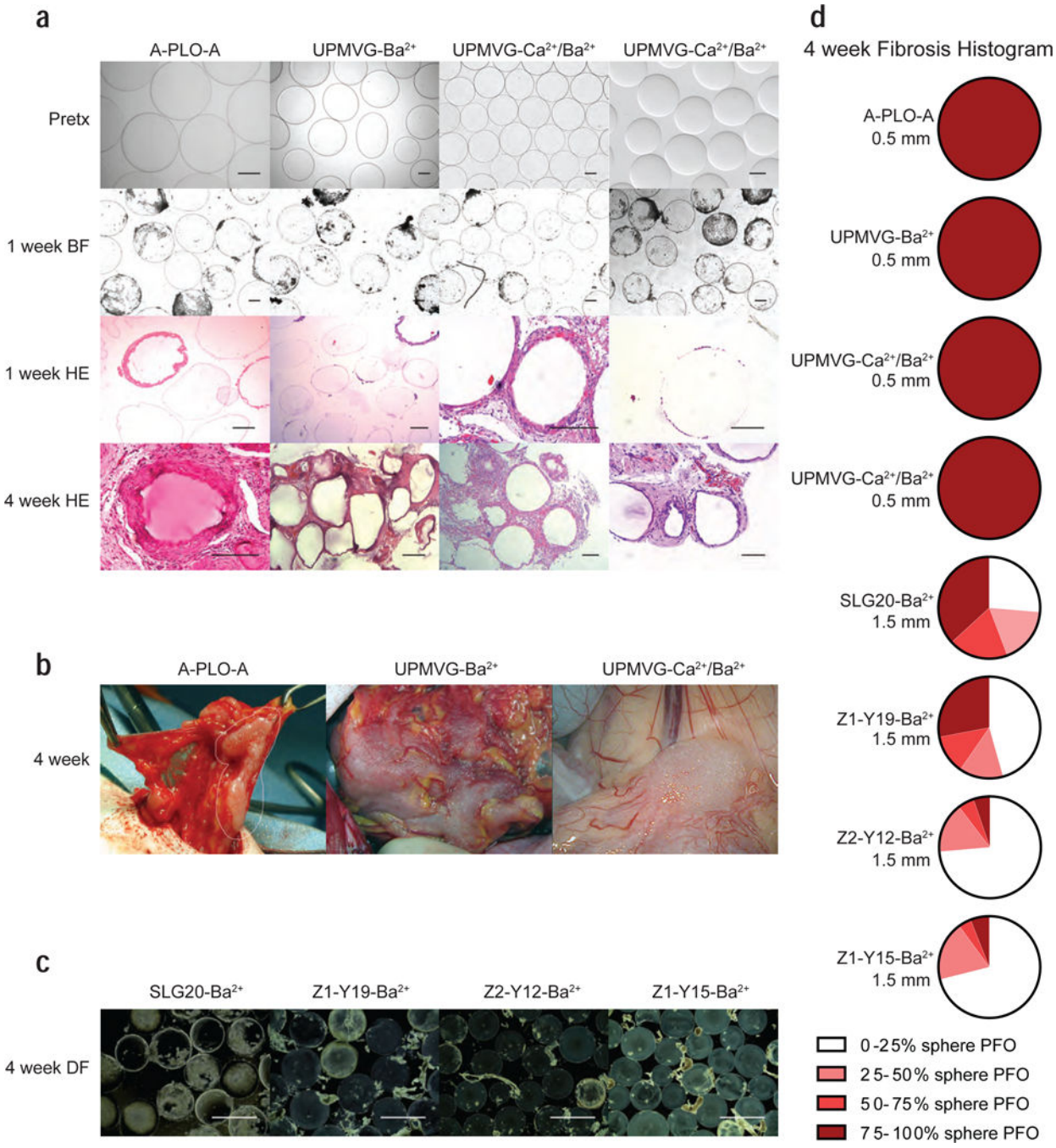

Figure 1: Empty alginate spheres implemented in the clinical trials provoke a foreign body response and pericapsular fibrotic overgrowth (PFO) post-implantation in non-human primates (NHP). The foreign body response to alginate spheres in NHP is mitigated by chemically modified alginate derivatives.

(a) Representative images of the three clinical alginate sphere formulations sized 0.5 mm post IP implantation in NHP. These were the same sphere formulations (A-PLO-A, UPMVG-Ba^{2+}, UPMVG-Ca^{2+}/Ba^{2+}) implemented in the clinical trials with transient encapsulated islet graft function. Each column of images depicts representative bright-field performed pre-transplantation; bright-field and H & E stained sections of spheres retrieved

Author Manuscript Author Manuscript Author Manuscript Author Manuscript

at 1 week; and H & E stained sections of omental biopsies containing spheres taken at 4 weeks. (A-PLO-A: $n = 2$ baboons; UPMVG-Ba^{2+}: $n = 1$ baboon; UPMVG-Ca^{2+}/Ba^{2+}: $n = 2$ baboons (left) and $n = 1$ cynomolgus (right); scale bars = 0.2 mm). Due to vendor issues with continued procurement of baboons, studies were subsequently performed in cynomolgus macaques. UPMVG-Ca^{2+}/Ba^{2+} formulations were implanted into both baboon and cynomolgus to verify the NHP species yield similar foreign body responses to the same alginate formulation. (b) Representative surgical images of A-PLO-A, UPMVG-Ba^{2+}, UPMVG-Ca^{2+}/Ba^{2+} adhered to omental tissue at 4 weeks. The spheres could not be removed by peritoneal lavage or mechanical agitation (left and center). Sphere clumping and fibrosis in the Douglas space (near bladder) was observed during retrieval from cynomolgus (right). (c) Representative dark-field images of SLG20-Ba^{2+} alginate spheres and three chemically modified alginate derivative spheres sized 1.5 mm retrieved at 4 weeks. (SLG20-Ba^{2+} $n = 1$ cynomolgus; Z1-Y19-Ba^{2+}; Z2-Y12-Ba^{2+}; Z1-Y15-Ba^{2+}; $n = 3$ cynomolgus per group; scale bars = 2 mm; *). (d) Histograms depict the average degree of PFO for the empty sphere retrievals performed at 4 weeks for each sphere formulation tested in NHP (A-PLO-A, UPMVG-Ba^{2+}, UPMVG-Ca^{2+}/Ba^{2+}, SLG20-Ba^{2+}, Z1-Y19-Ba^{2+}, Z2-Y12-Ba^{2+}, Z1-Y15-Ba^{2+}). Retrieved spheres were categorized by the percent of sphere surface area coverage by PFO; 0 <25%, 25–50%, 50–75%, 75–100% total surface area coverage by PFO. The pie sections depict the average percentage of spheres assessed in each category for each NHP sphere cohort. White and light colors depict little sphere coverage by fibrosis and dark red colors depict spheres mostly fibrosed. Diameter of the sphere formulations is depicted in the figure. For the clinical trial sphere formulations, A-PLO-A, UPMVG-Ba^{2+}, UPMVG-Ca^{2+}/Ba^{2+}, very few spheres were retrieved at 4 weeks so histograms are depicted as mostly fibrosed dark red. (SLG20-Ba^{2+}: $n = 95$ spheres assessed from 1 NHP; Z1-Y19-Ba^{2+}: $n =$ 143, 76, 68 spheres assessed from 3 NHP; Z2-Y12-Ba^{2+}: $n = 174$, 129, 125 spheres assessed from 3 NHP; Z1-Y15-Ba^{2+}: $n = 84$, 120, 64 spheres assessed from 3 NHP). * Note data presented for empty SLG20-Ba^{2+}, Z1-Y19-Ba^{2+}, Z2-Y12-Ba^{2+}, Z1-Y15-Ba^{2+} are from unpublished results within NHP cohorts for data sets collected in previously published reports[26,27].

Author Manuscript Author Manuscript Author Manuscript Author Manuscript

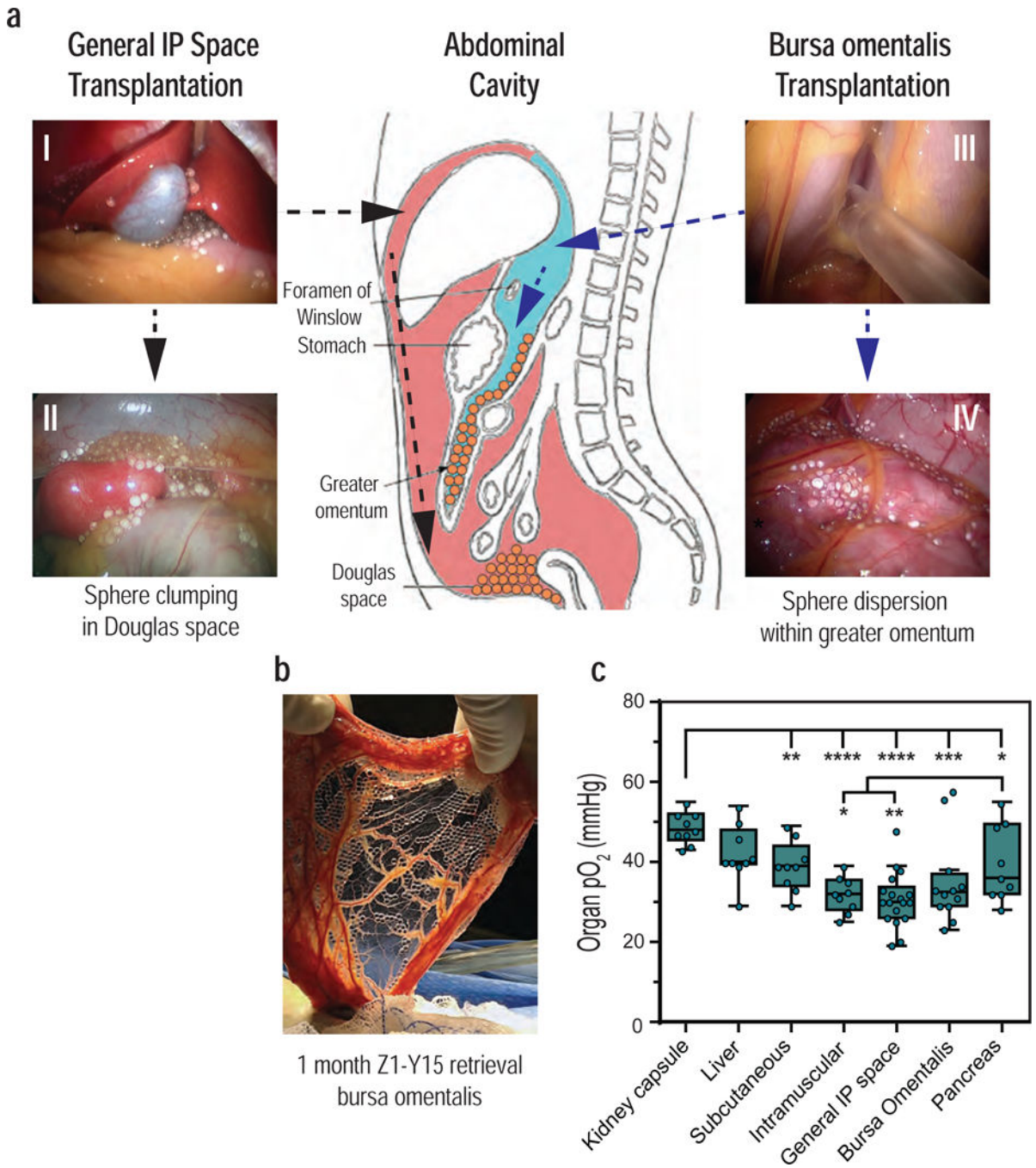

Figure 2: Transplantation method (general IP space vs. bursa omentalis) causes differential spatial distribution of the Z1-Y15 alginate spheres post-implantation.

(a) *General intraperitoneal space transplantation*: Z1-Y15 spheres were laparoscopically distributed around the left and right medial lobes of the liver within the intraperitoneal space (pink) (I). At 1-month post-implantation, the non-fibrosed spheres had settled and clumped within the Douglas space (II). *Bursa omentalis transplantation*: the stomach was lifted with a laparoscopic grasper and a small incision was made into an avascular section of the gastrocolic ligament. The Z1-Y15 spheres were then infused into the bursa omentalis (blue) (III). At 1-month post-implantation, the Z1-Y15 spheres remained spatially dispersed within

Author Manuscript Author Manuscript Author Manuscript Author Manuscript

the bilayer of the greater omentum (IV). A schematic of the two transplantation methods provides the location of the anatomical sites and a summary of the spatial distributions of the Z1-Y15 spheres during the 1-month retrievals (center). The general IP space transplantation was repeated independently for n = 10 NHP and the bursa omentalis transplantation for n = 7 NHP with resultant similar spatial distributions. Anatomical schematic adapted from original work created by Cuneyt Kayaalp[67] (b) The greater omentum was extracted through the supra umbilical midline incision at 1 month and shows translucent, unattached Z1-Y15 spheres with encapsulated allogeneic islets within the omental tissue bilayer. Sections of the greater omentum were excised to flush out encapsulated allogenic islets free of PFO depicted in Figure 3. (c) Partial oxygen pressures (pO_2) of various transplantation sites that have been previously investigated for encapsulated islet transplantation. The kidney capsule has the highest pO_2 measurements compared to the other anatomical sites. The intramuscular space (rectus abdominis) and general IP space have lower pO_2 compared to the pancreas, liver, subcutaneous and kidney capsule. The bursa omentalis site was not found to be statistically significantly different than the pancreas or the general IP space. (* $p <$ 0.05; individual p values given in supplementary table 3; one-way analysis of variance (ANOVA) with Fisher's LSD for multiple comparisons; 3 steady-state measurements were taken for each anatomical site from the same primate; $n = 3$ NHP; box and whisker with median, upper and lower quartile ranges, outliers, 1.5× IQR, individual data points overlaid).

Author Manuscript Author Manuscript Author Manuscript Author Manuscript

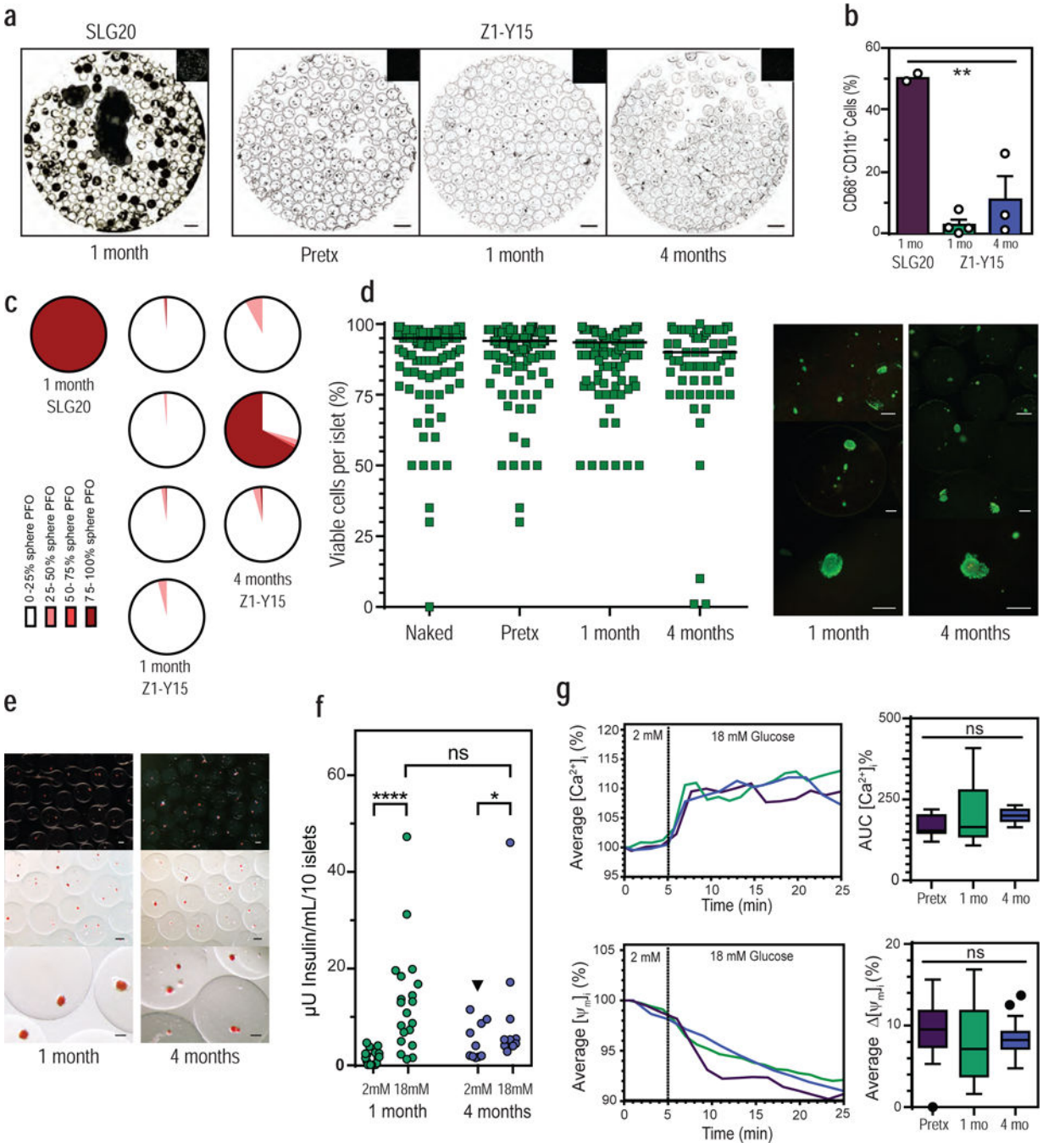

Figure 3: Z1-Y15 alginate protects viable and glucose responsive allogeneic islets in non-human primates without any immunosuppression.

(a) Representative inverted phase contrast of retrieved spheres: SLG20 empty spheres at 1 month, Z1-Y15 spheres with encapsulated allogeneic islets pre-transplantation (pretx), post retrieval from NHP at 1 month, and 4 months. (b) Percentages of $CD68^+/CD11b^+$ macrophage populations dissociated from retrieved sphere surfaces using flow cytometry (** $p = 0.0013$; one-way analysis of variance (ANOVA) with bonferroni multiple-comparison correction; SLG20 $n = 2$ NHP; Z1-Y15 1 month $n = 4$ NHP; Z1-Y15 4 month $n = 3$ NHP; mean ± SEM; individual data points overlaid). (c) Histograms depict the degree of

Author Manuscript Author Manuscript Author Manuscript Author Manuscript

PFO sphere coverage for each of the primate retrievals at 1 month (SLG20 and Z1-Y15) and 4 months (Z1-Y15) post-transplantation in NHP. White and light colors depict little sphere coverage by fibrosis and dark red colors depict spheres mostly fibrosed. The SLG20 spheres with encapsulated islets were completely adhered to omental tissue and are depicted as mostly fibrosed dark red. (Z1-Y15 encapsulated islets at 1 month: 121, 90, 152, and 125 spheres assessed from $n = 4$ NHP; Z1-Y15 encapsulated islets at 4 months: 160, 167, and 128 spheres assessed from $n = 3$ NHP). (d) Estimated percentages of viable cells within islet cell clusters following live/dead staining performed pre-encapsulation (naked), post-encapsulation in Z1-Y15 alginate (pretx), and post retrieval of non-fibrosed spheres at 1 month and 4 months (naked: $n = 144$ total islets assessed, median viability 95.0%; post-encapsulation (pretx): $n = 191$ total islets, median viability 94.0%; Z1-Y15: 1 month retrieval: $n = 133$ total islets over 4 NHP retrievals, median viability 93.5%; Z1-Y15: 4 month retrieval: $n = 69$ total islets over 2 NHP, median viability 90.0%; 25–50 islets were scored per primate; median value per group depicted). Viability scores were analyzed using the Wilcoxon signed rank test to assess whether median viability was significantly different from 75%. Seventy-five percent was chosen as the biological reference because it is the cutoff for islet preparations suitable for clinical intraportal islet transplantation. Six out of seven encapsulated islet preparations demonstrated significantly higher viability than 75% from pre-encapsulation (naked), post-encapsulation (pretx), to post retrieval from NHP ($p < 0.05$; Wilcoxon signed rank test; two tailed; individual p values presented in supplementary table 6). One primate retrieved at 4 month presented with fibrosis and non-viable islets. Representative fluorescent images of retrieved Z1-Y15 encapsulated allogeneic islets with live/dead stains fluorescein diacetate (FDA) and propidium iodide (PI) at 1 month and 4 months. (e) Retrieved Z1-Y15 encapsulated allogeneic islets at 1 month and 4 months stained with the red dye dithizone for macroscopic detection of mature insulin granules within engrafted endocrine tissue (representative of the n = 6/7 retrieved NHP). (f) Glucose stimulated insulin secretion of viable retrieved Z1-Y15 encapsulated allogeneic islets showing secreted insulin levels per 10 islets when incubated in a low glucose solution (2 mM glucose) for 1 hour and high glucose solution (18 mM glucose) for 1 hour. The Z1-Y15 spheres with encapsulated allogeneic islets samples secreted higher levels of insulin under high glucose compared to low glucose at 1 and 4 months retrievals. Insulin levels under low glucose were significantly higher when comparing 1 month and 4 month retrievals (black triangle $p = 0.01$), yet high glucose insulin levels were not significant when comparing 1 month and 4 months ($p = 0.21$). ($****$ $p < 0.0001$; * $p = 0.03$; Wilcoxon matched-pairs signed-rank test (comparing low to high at 1 month and 4 months); unpaired Mann-Whitney test (comparing lows or highs at 1 month and 4 months); both two-tailed; 1 month: $n = 4$–6 replicates of 10 islets per n = 4 independent NHP retrievals, n = 19 total samples; 4 month: $n = 5$ replicates of 10 islets per $n = 2$ independent NHP retrievals; n = 10 total samples, individual data points shown). (g) Average islet traces of intracellular calcium influx ($[Ca^{2+}]_i$) and mitochondrial potential changes ($\Delta\Psi_m$) of Z1-Y15 spheres with encapsulated allogeneic islets in response to a perifusion based glucose challenge (left column). Assessments were performed pre-transplantation, post 1 month retrieval, and post 4 month retrieval. Average AUC $[Ca^{2+}]_i$ % of intracellular calcium influx during time of 18 mM glucose stimulus (5–25 min) (top right). Average percent decrease in mitochondrial potential changes ($\Delta\Psi_m$ % change) after response to 18 mM glucose stimulus at 25 min (bottom

right). (ns $p > 0.05$; one-way analysis of variance (ANOVA); pre-transplantation: $n = 31$ individual islets assessed; 1-month retrieval: $n = 17$ individual islets; 4-month retrieval: $n = 20$ individual islets; box and whisker with median, upper and lower quartile ranges, outliers, and 1.5× IQR).

Author Manuscript Author Manuscript Author Manuscript Author Manuscript

Author Manuscript Author Manuscript Author Manuscript Author Manuscript

Table 1:

Characteristics of empty alginate sphere formulations implanted into the general IP space of NHP

Sphere Formulation	Clinical Trial Reference	Polymers	Crosslinking Formulation	Microsphere Diameter (mm)	Dose transplanted per NHP (volume caps/NHP weight)
A-PLO-A spheres	**Calafiore et al** [12,13] **2006, 2011; 4 patients**	1.7% custom-made highly purified alginate poly-L-ornithine (PLO)	109 mM Ca^{2+} PLO double coat 0.10% (10 min) 0.05% (6 min) 0.17% alginate final coat	0.5	Baboon (*n* = 2) 4mL/kg
UPMVG-Ba^{2+} spheres	**Tuch et al** [14]; **2009; 4 patients**	2.2% UPMVG alginate "ultra pure medium viscosity high guluronic acid content"	20 mM Ba^{2+}	0.5	Baboon (*n* = 1) 2 mL/kg
UPMVG-Ca^{2+}/Ba^{2+} spheres	**Pipeleers et al** [15]; **2013; 1 patient**	1.8% UPMVG alginate	50 mM Ca^{2+} 1 mM Ba^{2+}	0.5	Baboon (*n* = 2) 2 mL/kg Cynomolgus (*n* = 1) 1.5 mL/kg
SLG20-Ba^{2+} spheres	-	1.4% SLG20 alginate "sterile low viscosity high guluronic acid content"	20 mM Ba^{2+}	1.5	Cynomolgus (*n* = 1) 3 mL/kg
Z1-Y19-Ba^{2+} spheres	-	5% UPVLVG-(Z1-Y19) "ultra pure very low viscoscity high guluronic acid content + Z1-Y19 small molecule" 3% SLG100 "sterile medium viscocity high guluronic acid" 70:30 Blend	20 mM Ba^{2+}	1.5	Cynomolgus (*n* = 3) 3 mL/kg
Z2-Y12-Ba^{2+} spheres	-	5% UPVLVG-(Z2-Y12) 3% SLG100 70:30 Blend	20 mM Ba^{2+}	1.5	Cynomolgus (*n* = 3) 3 mL/kg
Z1-Y15-Ba^{2+} spheres	-	5% UPVLVG-(Z1-Y15) 3% SLG100 70:30 Blend	20 mM Ba^{2+}	1.5	Cynomolgus (*n* = 3) 3 mL/kg